AUGUST 10 2026

Acoustic transfer functions for tire/road noise prediction through equivalent monopole sources: Numerical modelling and experimental validation

Samanta Dallasta ; Luca Rapino ; Francesco Ripamonti ; Simone Baro ; Roberto Corradi

J. Acoust. Soc. Am. 160, 1240–1251 (2026)
https://doi.org/10.1121/10.0044578

JASA ARTICLE

Acoustic transfer functions for tire/road noise prediction through equivalent monopole sources: Numerical modelling and experimental validation

Samanta Dallasta,[1,a)] Luca Rapino,[2] Francesco Ripamonti,[1] Simone Baro,[2] and Roberto Corradi[1]
[1]Department of Mechanical Engineering, Politecnico di Milano, Milano 20156, Italy
[2]Pirelli Tyre S.p.A., Milano 20156, Italy

ABSTRACT:
Previous research has shown that tire noise can be modelled through equivalent monopoles and acoustic transfer functions (ATFs). In this study, the numerical modelling of ATFs and their use for the prediction of tire/road noise is investigated as an alternative to ATFs derived from experimental measurements, aiming to reduce the experimental effort required during testing campaigns. Numerical models are developed to reproduce the acoustic characteristics of the environments where tire/road noise tests are conducted, both indoor and outdoor. To assess the reliability of the simulations in representing the actual acoustic propagation conditions, the computed ATFs are validated against experimental measurements. The numerical transfer functions are then employed for the synthesis of equivalent monopoles and for the prediction of coast-by noise levels. The predicted results are finally compared with experimental coast-by data to evaluate the accuracy of the proposed approach.
 https://doi.org/10.1121/10.0044578

(Received 18 March 2026; revised 20 June 2026; accepted 16 July 2026; published online 10 August 2026)

[Editor: Michael J. White] Pages: 1240–1251

I. INTRODUCTION

Tire/road noise is the sound generated by the interaction between a rolling tire and a road surface (Li, 2018; Sandberg and Ejsmont, 2002). At standard driving speeds (above 25–30 km/h), it becomes the main contributor to road traffic noise for passenger cars, exceeding engine noise (Campello-Vicente *et al.*, 2017; Sandberg, 2001). The significance of tire/road noise has become even more important with the growing market of electric vehicles, which represented over one in five cars sold globally in 2024 (IEA, 2025). Scientific literature has linked long-term exposure to traffic noise with higher risks of cardiovascular diseases, sleep disturbances, and chronic stress (Dratva *et al.*, 2012; Song *et al.*, 2026). The growing awareness of the harmful effects of traffic noise on human health has motivated the enforcement of mitigation measures. The European Union (EU) has introduced increasingly demanding requirements on the noise emissions of vehicles, driving the automotive industry, and also tire manufacturers, to develop quieter solutions. To provide consumers with transparent information and the ability to compare tires based on key factors, the acoustic performance of tires is certified through a labelling system. Tire labelling is regulated through Regulation (EU) 2020/740 (EU, 2020), which defines the criteria for measuring and classifying noise emissions. The noise parameter reported on the label is evaluated through the so-called coast-by test, standardized in United Nations Economic Commission for Europe Regulation No. 117 (European Commission, 2011). The resulting value is expressed in decibels, and it is compared with reference thresholds to assign a noise class shown with a letter rating.

The ability to accurately model the noise emitted by tires represents an advantage during the design phase. Reliable modelling would, in fact, reduce the need for numerous prototypes and consequently lower the costs associated with experimental campaigns. However, tire/road interaction is highly complex. Tire/road noise arises from different mechanisms, including vibroacoustic mechanisms (e.g., tread impact, texture impact), adhesion-related phenomena (stick-slip, stick-snap), and aeroacoustic effects (air pumping and turbulence) (Eisenblaetter *et al.*, 2010; Kim *et al.*, 2006; Li, 2018, 2019; Sandberg and Ejsmont, 2002; Wang, 2020; Winroth *et al.*, 2017). In addition to these generation mechanisms, amplification mechanisms (i.e., pipe and Helmholtz resonances and horn effect) also play a role (Lui and Li, 2004; Li, 2018; Rapino *et al.*, 2024a; Schutte *et al.*, 2015). Each mechanism acts over different frequency ranges and often overlaps with others, increasing the complexity of their analysis and modelling. These aspects are further complicated by the challenges of modelling the tire's nonlinear behaviour (Behnke and Kaliske, 2015; Meschke *et al.*, 1997).

Various approaches have been proposed in the literature for modelling tire/road noise. Numerical models offer high accuracy as they allow a detailed representation of both the tire structural response and the acoustic propagation of sound in air. Finite element method (FEM) and boundary

[a)]Email: samanta.dallasta@polimi.it

element method (Ding and Wang, 2019; Kim *et al.*, 2023; Kropp *et al.*, 2012; Nakajima *et al.*, 1993; Saraswat *et al.*, 2022) are frequently combined to perform full vibroacoustic simulations. These models usually imply high computational cost, are highly sensitive to input data, and present difficulties in realistically representing the complexity of the phenomena involved. Alongside purely numerical approaches, hybrid methods that combine simulations with experimentally calibrated inputs may be adopted. Representative examples include the HyRoNE and SPERoN models (Beckenbauer *et al.*, 2008; Klein *et al.*, 2008), which exploit hybrid numerical-experimental strategies to improve the accuracy of tire/road noise predictions. However, they require large datasets to calibrate the regression model. In addition to these approaches, a well-established methodology relies on the use of equivalent sources. In the literature, several studies have shown that monopoles can effectively represent complex acoustic fields. In these methods, by replacing tire noise sources with a set of equivalent monopoles, it is possible to achieve a significant simplification of the phenomena while maintaining good accuracy (Bécot, 2003; Lafont *et al.*, 2019). The strengths of these equivalent sources are identified by solving an inverse problem. This procedure requires sound pressure data obtained at selected receiver positions, either in the near-field or in the far-field, together with source-receiver acoustic transfer functions (ATFs). The sound pressures can be obtained from numerical simulations or experimental measurements. When the latter are employed, they are typically carried out in semi-anechoic chambers, where the controlled conditions ensure high repeatability and eliminate the influence of external environmental factors. An additional advantage of using experimental data is the possibility of bypassing potential inaccuracies associated with the numerical modelling of tire rolling noise generation mechanisms. In the same way, the ATFs can be determined either experimentally using an acoustic source (Dallasta *et al.*, 2025, 2026; Lafont *et al.*, 2019; Papaioannou *et al.*, 2020) or numerically (Dallasta *et al.*, 2024; Huijssen *et al.*, 2010; Rapino *et al.*, 2024b) through simulation. Moreover, after having identified the equivalent sources, they can be used to predict coast-by noise levels following the methodology presented by the authors in Dallasta *et al.* (2026).

This work addresses the numerical modelling of ATFs for tire/road noise prediction within the framework of the equivalent source method, with particular focus to the influence of modelling assumptions on the overall prediction chain. In contrast to the approaches presented by the authors in Dallasta *et al.* (2025, 2026), in this paper, ATFs are obtained through numerical simulations rather than direct measurements to reduce the need of dedicated and time-consuming experimental campaigns. A central aspect, however, is that the present work still relies on experimental data to confirm the robustness of the methodology. Indoor simulations are performed by reproducing the geometry of the deformed tire and the drum setup used in semi-anechoic chamber tests. The resulting numerical ATFs are assessed through comparison with measurements obtained using an omnidirectional source (QSource). Furthermore, a different model for the outdoor coast-by condition is developed. In this case, ATFs are again computed numerically with a model that accounts for the vehicle geometry and verified through dedicated measurements. Once validated, the indoor numerical ATFs are used to identify the equivalent sources by solving the inverse problem using sound pressure data from rolling tests carried out on a drum covered with a road surface replica. Finally, the synthesized sources in indoor environment are combined with the outdoor ATFs to simulate coast-by noise, reproducing the relative motion between tire and receiver, and the result of the prediction is compared with experimental data. This approach is intended to reduce the complexity of the experimental campaigns by eliminating the need for the measurement of the ATFs. In this context, the proposed framework enables us to assess how replacing measured ATFs with numerically obtained ones affects each stage of the prediction workflow, including indoor source identification and outdoor propagation.

The paper is organized as follows (Fig. 1). In Sec. II, the indoor numerical model is presented. Section III describes the outdoor numerical model. Section IV focuses

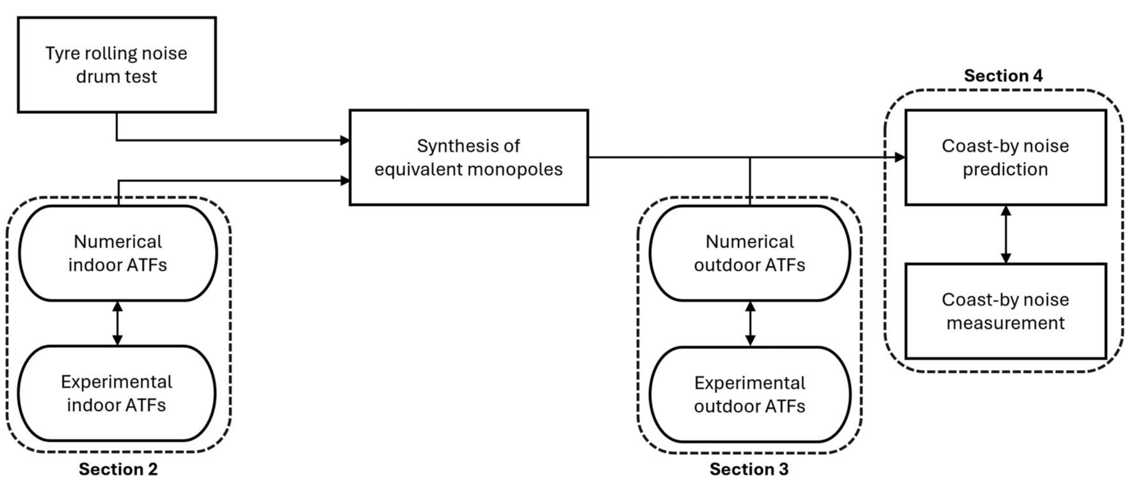

FIG. 1. Flowchart illustrating the approach and the contents of this work.

on the application of the computed ATFs for source synthesis and coast-by prediction. Section V concludes this study.

II. MODELLING OF THE INDOOR ACOUSTIC TRANSFER FUNCTIONS

The equivalent source methodology is a useful technique for representing complex acoustic sources through simplified equivalents, such as monopoles. The identification of these monopoles relies on two key elements: the knowledge of the sound radiated by the source at specific receiver locations and the corresponding source-receiver transfer functions.

A previous work by the authors (Dallasta *et al.*, 2025) presented an experimental approach in which both transfer functions and tire rolling noise measurements were performed. The two datasets were combined to solve the inverse problem, leading to the identification of the source strengths of the equivalent monopoles. Consequently, the transfer functions were not affected by possible approximations arising from the use of a numerical model since they were directly measured. The results confirmed the reliability of the method; nonetheless, it also highlighted that the measurement of ATFs for each source is considerably more demanding than the rolling tire test, as they require repeated measurements for each monopole location and careful positioning for every source-receiver transfer path. In the present work, tire rolling noise measurements are still employed, whereas the ATFs are computed using a numerical model of the indoor testing environment. This approach aims at significantly reducing the complexity of the experimental campaign, avoiding the need to measure transfer functions. While the development of the numerical models requires an initial effort for geometry reconstruction and calibration of the propagation environment, this step is intended to be performed once within the proposed workflow. The resulting models are reusable and can be applied to multiple tire configurations without the need for repeated ATF measurement campaigns, shifting part of the effort from experiments to simulation while increasing overall flexibility.

As part of the development of the indoor model for ATF simulation and the measurement of radiated noise from the rolling tire, indoor tests were carried out in the semi-anechoic chamber at Pirelli's facility in Breuberg, Germany. The tire test rig consists of a turret on which the tire is mounted. The tire is then loaded against a 2-m diameter drum covered with road surface replica of an International Standardization Organization (ISO) 10844 (ISO, 2021) outdoor test track. The semi-anechoic test rig is shown in Fig. 2.

Two arrays of 1/2-in. microphones were employed to measure the sound field (Fig. 3). The first array, consisting of 21 microphones, was arranged in a circular arc spanning 210° at a radius of 1.5 m from the centre of the tire footprint (blue circles). The microphones were positioned at a height of 0.30 m above the ground with a nominal angular spacing of 10°, except between microphones 10–11 and 11–12, where a 15° spacing was adopted. This array, positioned in the far-field region within the frequency range of interest (450–2820 Hz), was used to synthesize the equivalent sources representative of tire/road noise in the tested conditions. A second linear array of 19 microphones was additionally used, located 2 m away from the drum and extending 5.3 m in length (red circles). The microphones of the linear array were positioned at a height of 0.32 m above the ground and were equally spaced along the array length. These microphones were not involved in the synthesis process but were used to provide an independent validation of the methodology in indoor conditions.

Two sets of measurement were performed. On the one hand, rolling noise data were collected using a 225/45R17 tire rotating in clockwise direction at a constant speed of 80 km/h on the asphalt replica, under a vertical load of 450 kg and with an inflation pressure of 2.2 bar. On the other hand, ATFs measurements were performed to validate the developed numerical model by assessing its reliability and identify possible discrepancies. The dedicated experimental campaign conducted to acquire the ATFs followed the methodology outlined in Dallasta *et al.* (2025). Under static tire conditions, the setup employed a Qsource (Siemens Q-MHF; Siemens, Munich, Germany), an omnidirectional acoustic source that also allows the measurement of the emitted volume acceleration through an internal sensor. Together with the sound pressure recorded by the microphones, these measurements enabled the evaluation of the experimental ATFs.

FIG. 2. Tire test rig used for indoor noise measurements in the semi-anechoic chamber.

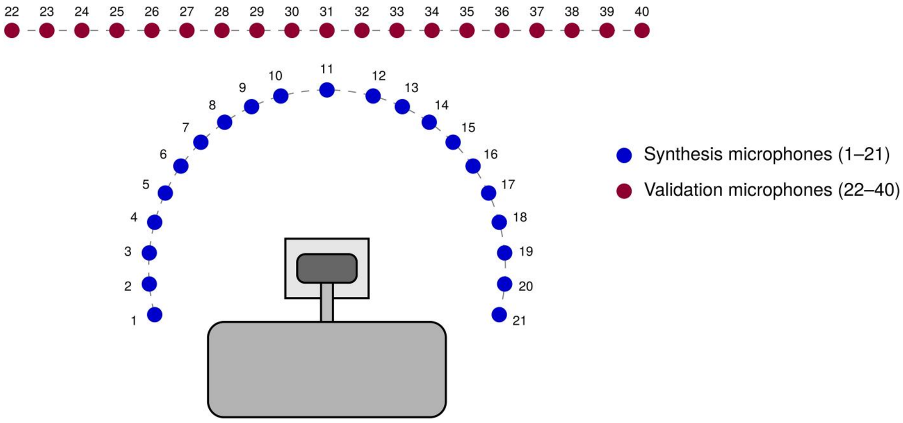

FIG. 3. Experimental setup for measuring the noise radiated by the rolling tire.

The numerical model replicating the acoustic conditions of the indoor environment was developed. A CAD representation of the rig was created. Based on its geometry, an acoustic finite element model was built in the acoustic FEM software Wave6 (Fig. 4). Furthermore, the tire was included into the model in its static and deflected configuration, accounting for the acoustic amplifications determined by the horn-shaped cavity of the tire and the air volumes within the tire grooves. The wheel rim geometry was represented by a simplified axisymmetric surface resembling its outer profile, without modelling the spokes and the hub. The acoustic domain was discretized and, to complete the air volume definition, the free-field condition was included by means of a perfectly matched layer (PML). An adaptive mesh approach was used, imposing wavelength-dependent meshing criteria to satisfy frequency-resolution requirements while reducing computational costs. Finally, the test-rig surfaces were described in terms of their acoustic properties, with the tire being considered as acoustically rigid.

To obtain the ATFs, both microphones and monopole sources were included in the numerical model. In particular, 14 monopole sources were placed around the tire footprint based on prior experimental findings indicating that tire/road noise is primarily associated with the contact area. The number and distribution of monopoles were selected based on the inverse problem formulation and the frequency range of interest, ensuring an overdetermined system and adequate spatial sampling of the dominant radiation regions of the tire, with a spacing consistent with the wavelength at the highest analyzed frequency. The same strategy was adopted in the previous study (Dallasta *et al.*, 2025), which showed good agreement in the frequency range of interest between predicted and measured sound pressure levels under indoor conditions when using experimental ATFs. Inside the model, the same microphones used in the physical tests were included to obtain monopole responses. The transfer functions were calculated by activating each monopole individually with a broadband unitary volume acceleration, thus linking the *i*th monopole input to the *j*th receiver output.

For the comparison between experimental and numerical ATFs, Figs. 5–7 show the ATFs for single monopoles positioned in the trailing edge, sidewall, and leading edge regions of the tire, respectively. The terms "leading edge" and "trailing edge" clarify the monopole positions relative to a tire rotating clockwise, although all measurements were conducted with the tire in a static condition. Overall, the comparison shows good agreement in terms of directivity pattern. Higher values are consistently observed in the direction facing the monopole, while microphones on the opposite side register lower values due to acoustic shadowing by

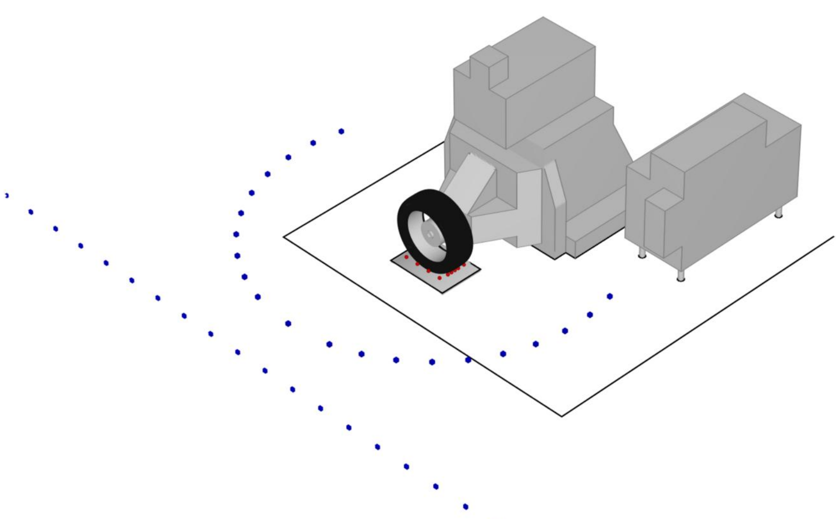

FIG. 4. Acoustic finite element model of the semi-anechoic chamber and tire testing rig.

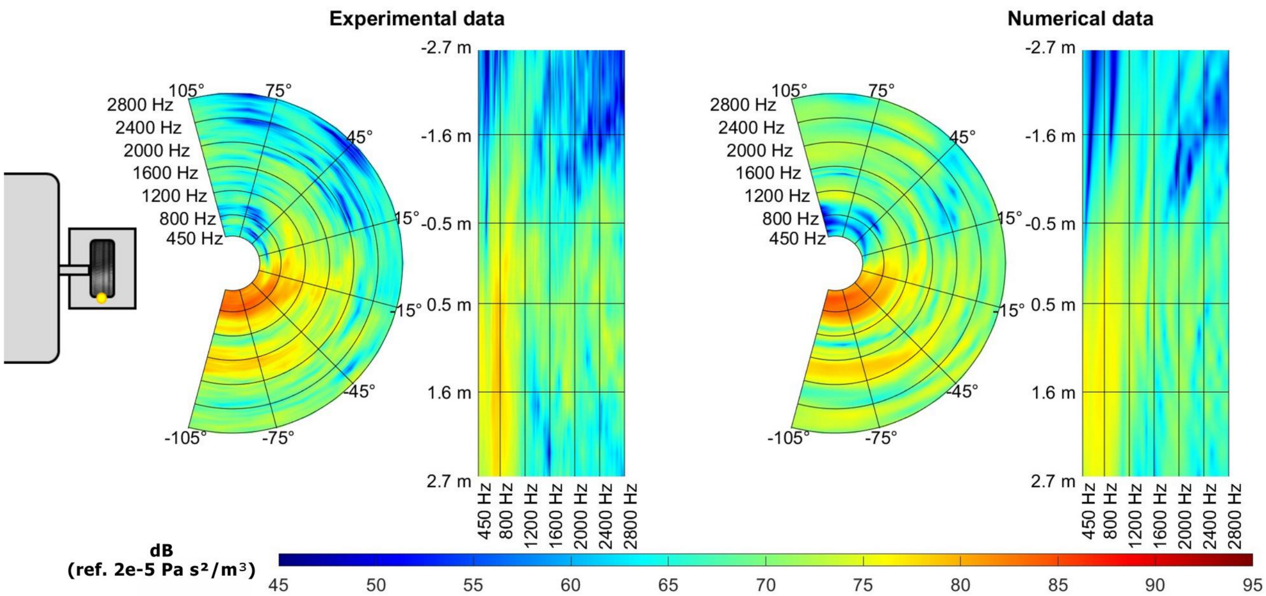

FIG. 5. Comparison between experimental and numerical ATFs for a monopole located in the trailing edge region of the tire. Results are shown for the 21 microphones of the circular array and the 19 microphones of the linear array.

the tire. For example, a monopole in the leading edge region produces higher responses at microphones located on the same side, while those on the trailing edge and sidewall sides are partially shielded. The difference between numerical and experimental ATFs is evaluated by averaging the ATFs over either the semi-circular or radial microphone arrays, resulting in an average error in overall levels of −1.5 dB for the radial array and −2.7 dB for the linear array. It is worth noting that accurately modelling these acoustic environments is inherently challenging, as deviations in geometry, boundary conditions, or material properties influence the outcomes of the numerical simulation. In particular, main differences appear at high frequencies, where acoustic modelling is affected by the need for finer geometric resolution, the increased sensitivity of the acoustic field to reflections and diffraction, and the greater difficulty in accurately representing the acoustic properties of materials.

To highlight overall trends, Fig. 8 shows the averaged ATFs. The averaging was carried out by simultaneously activating the monopoles belonging to the leading edge, trailing edge, or sidewall regions as if they were driven by unit incoherent sources and by considering the average sound pressure levels measured at the microphones directly facing those regions, both for the experimental (black line) and numerical ATFs (blue line). In addition, to justify the need for a detailed ATF simulation, an analytical model was introduced (red line), based on the image source method. For the latter, the monopoles Green's functions account

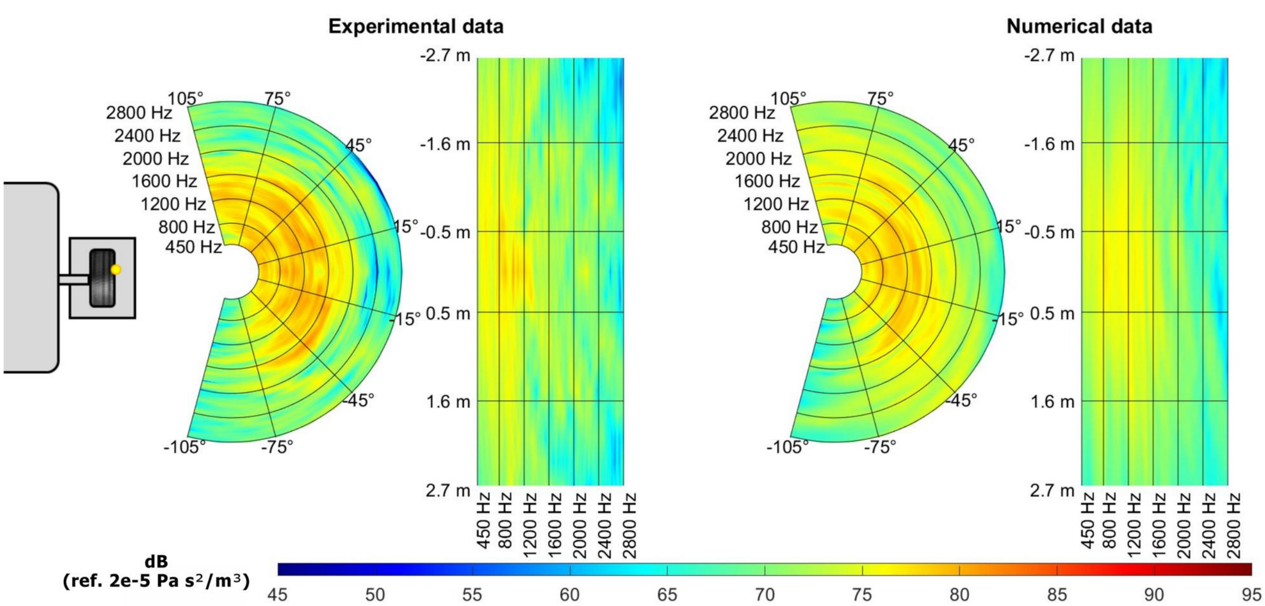

FIG. 6. Comparison of experimental and numerical ATFs, as in Fig. 5, for a monopole in the sidewall region of the tire.

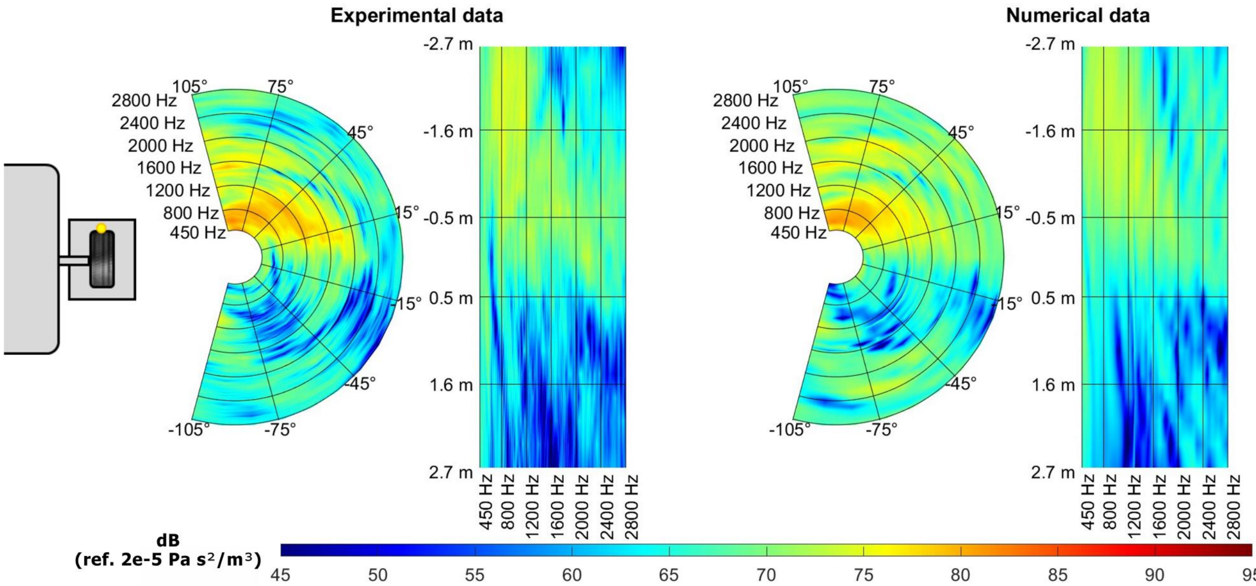

FIG. 7. Comparison of experimental and numerical ATFs, as in Fig. 5, for a monopole in the leading edge region of the tire.

only for a reflective ground (plane) to approximate boundary effects. This approach fails to reproduce the amplification phenomena observed in the real environment, resulting in noticeable discrepancies with respect to the measurements. This outcome highlights the importance of accurately modelling the acoustic environment, with the numerical simulation showing a good overall agreement with the experimentally measured source-receiver transfer functions. The leading and trailing edge regions also exhibit the effect of the horn amplification attributed to the tire geometry (Kropp *et al.*, 2000; Schutte *et al.*, 2015). Some differences can be observed between the transfer functions of the leading edge/trailing edge regions and those of the tire sidewall, which may be due to slight mismatches in the positions of the monopoles between the numerical model and the experimental measurements.

III. MODELLING OF THE OUTDOOR ACOUSTIC TRANSFER FUNCTIONS

The coast-by method for the measurement of tire-to-road sound emission is described in ISO 13325 (ISO, 2019). The test consists of measuring the vehicle's noise emission in non-powered operation, thereby excluding the contribution from a combustion engine. In this study, an electric vehicle was used, such that the measured noise corresponds

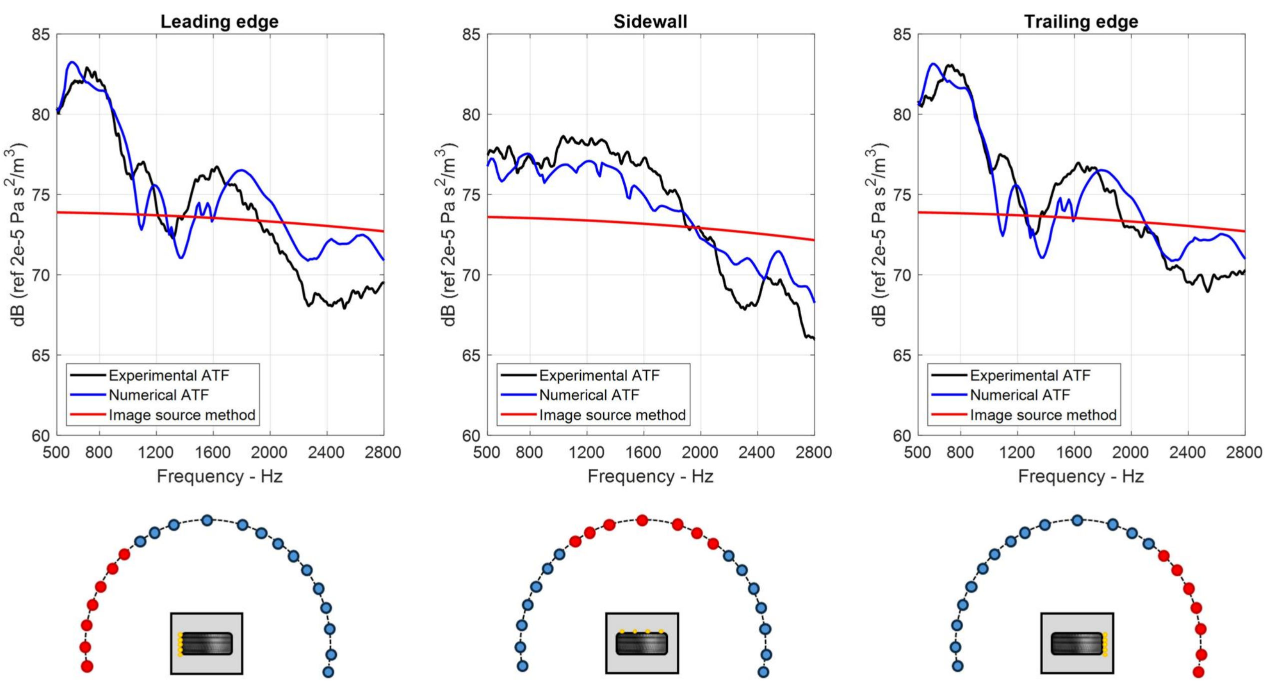

FIG. 8. Spatially averaged ATFs obtained by grouping monopoles and corresponding microphones in the leading edge, sidewall, and trailing edge regions.

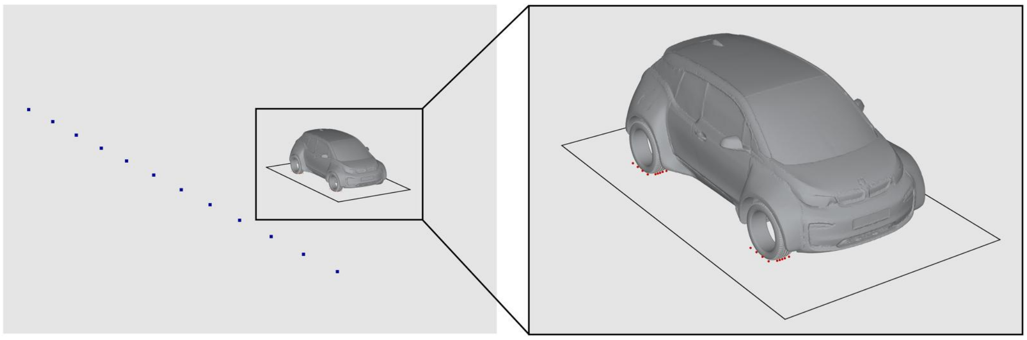

FIG. 9. Numerical model of the BMW i3 with mounted tires, and microphone locations (blue dots), with a zoomed-in view highlighting the monopole sources (red circles) around the tire footprint.

mostly to the contribution from tire/road interaction. Two microphones, positioned at 1.2 ± 0.02 m above the test area and 7.5 ± 0.05 m distance from the centreline of the track, are used for measuring sound pressure data as the vehicle travels along the track. In this work, the outdoor coast-by measurements were carried out on the test track in Vizzola Ticino, Italy, which complies with ISO 10844 (ISO, 2021) requirements for test track characteristics.

For coast-by predictions based on equivalent monopole sources, an outdoor model representative of real test conditions must be developed. The model must include the complete vehicle structure with the four mounted tires, as their presence influences the propagation paths and diffraction patterns of the sound field generated by the tires. In analogy with the indoor configuration, this approach ensures an accurate reproduction of the outdoor test track characteristics where coast-by measurements are performed. Since the outdoor tests were performed using a BMW i3 (BMW, Munich, Germany), the same vehicle was digitized using a laser scanner. Only the upper and lateral portions of the vehicle were scanned; the underbody was not captured and was included as a closed surface in the model. This procedure produced a geometric mesh consistent with the actual test vehicle (Rapino *et al.*, 2024b). For the acoustic simulation, the static vehicle geometry, including all four tires, was modelled (Fig. 9). The tire geometry accounted for the deformation under vertical loading on a flat surface, allowing accurate representation of the contact patch, while the tire rim, consistently with the indoor model, was not explicitly modelled. In particular, the geometrical details of the rim were considered to play a secondary role. The acoustic domain was discretized using a finite element pre-processor, with free-field conditions applied via an adaptive PML. Only a single array of microphones on the right side of the vehicle is considered in this study. To predict the sound radiated by the tires mounted on the moving vehicle, instead of simulating the vehicle's movement along the track, different positions occupied by the car in time were mapped by considering a linear array of receivers (Dallasta *et al.*, 2026). For this reason, a linear array of microphones must be included in the numerical simulation. In particular, 12 microphones were arranged in a linear array at a height of 1.2 m and a distance of 7.5 m from the centre of the track, with a uniform spacing of 2 m. The array is used to predict the sound radiated by simulating the relative motion of the vehicle with respect to the coast-by microphone during the test. Finally, the equivalent monopoles were included at the four corners (FR, front right; FL, front left; RR, rear right; RL, rear left), using the placement of the sources (Dallasta *et al.*, 2026) defined in indoor conditions.

The acoustic properties of the absorbing materials on the vehicle were not available. Therefore, all vehicle surfaces, including the underbody and the wheel arches, were modelled as acoustically perfectly reflective. Road surface absorption characteristics were also unknown; two limiting cases were considered to cover the possible acoustic effects: a non-absorbing surface with a ground absorption coefficient $\alpha = 0\%$ and a surface with $\alpha = 8\%$, corresponding to the maximum value specified by ISO 10844 (ISO, 2021) for the drive lane area. In both cases, a constant value was considered across the entire frequency range.

The developed model was used to compute the ATFs required for coast-by predictions. As with the indoor configuration, the numerical ATFs were first compared with experimental measurements. Experimental ATFs were collected at the same positions, using a Qsource with the vehicle centered on the track and monopoles placed at the same locations as in the numerical model. In this case, as well, the objective is to verify the differences between the numerical model and the experimental data before carrying out the coast-by simulation, thereby allowing the observation of the differences between the predictive model and the experimental data.

Figure 10 presents the comparison for four different monopole locations between experimental and numerical ATFs, considering the simulations with both $\alpha = 0\%$ and $\alpha = 8\%$, and showing the position of the vehicle with respect to the microphone array. Also, for the outdoor case, the difference between numerical and experimental ATFs is evaluated by averaging the transfer functions, and the resulting average errors in overall levels for the $\alpha = 0\%$ case and for the $\alpha = 8\%$ case are reported in Table I. The monopoles of the left and right sides of the vehicle are considered separately due to their distance from the microphone array, resulting in significant differences in amplitude levels. The best agreement is obtained for the $\alpha = 8\%$ case, which yields

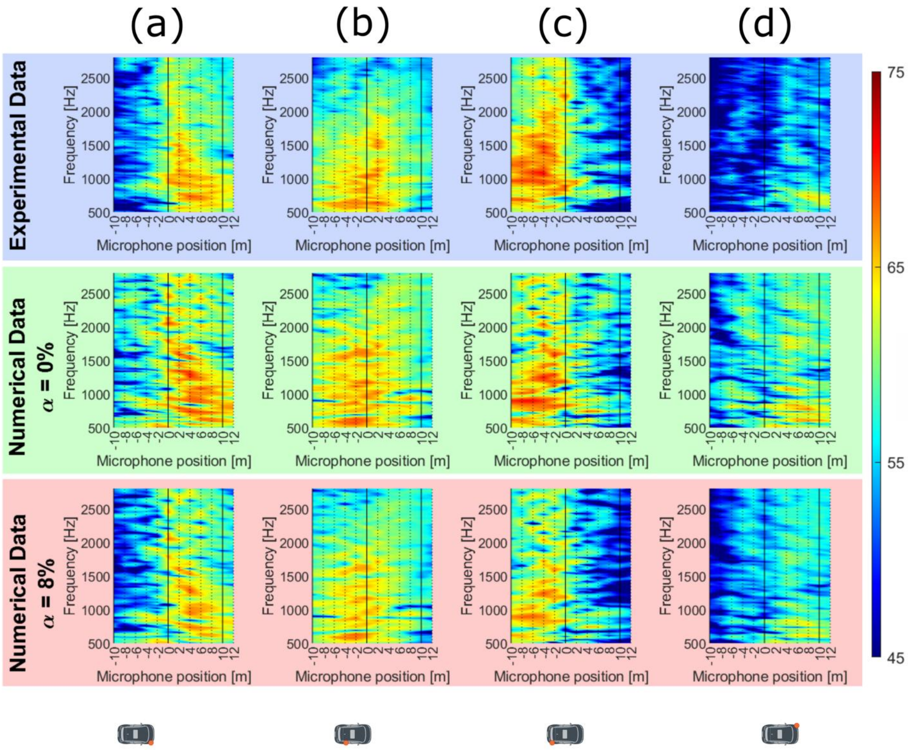

FIG. 10. Comparison of ATFs in terms of SPL across experimental (top row), numerical ATFs with $\alpha = 0\%$ (central row) and numerical ATFs $\alpha = 8\%$ (bottom row) for four different monopole locations [(a) FR leading edge monopole, (b) RR side monopole, (c) RR trailing edge monopole, (d) FL leading edge monopole]. Results are shown for the 12 microphones of the linear array.

lower errors. Overall, the numerical model captures the general behaviour of the experimental data, reproducing the main spatial and frequency-dependent patterns. As expected, higher ATF amplitudes are observed at microphones located closer to the monopole under consideration, consistent with basic acoustic principles. The influence of the tire is also evident. For example, in Fig. 10(c), where the monopole is positioned at the trailing edge on the RR corner, microphones in unobstructed positions exhibit higher amplitudes compared to those partially masked by the tire itself, highlighting the role of acoustic shadowing due to vehicle and tire geometries. This emphasizes the importance of including the tire deformed shapes and their position relative to the vehicle body in the model. It also demonstrates the limitations of modelling the environment by means of analytical hemi-free field space formulations.

Regarding the effect of the ground absorption coefficient, it can be observed that introducing acoustic absorption, as expected, generally reduces the amplitudes of the frequency response functions compared to the case of null absorption. Amplitude discrepancies are particularly noticeable at corners opposite the microphone array [Fig. 10(d), Table I], where the effect of the vehicle's presence is more evident and simplifications of the vehicle underbody have a greater influence than at corners on the same side as the array. However, monopoles farther from the array contribute less to the measured signal, so these mismatches are expected to have minimal impact on coast-by predictions.

TABLE I. Average overall error between numerical and experimental ATFs, reported for $\alpha = 0\%$ and $\alpha = 8\%$, separately for left- and right-side monopoles.

	Right-side monopoles	Left-side monopoles
$\alpha = 0\%$	1.1 dB	4.6 dB
$\alpha = 8\%$	−0.6 dB	1.9 dB

In order to further assess the comparison, Fig. 11(a) shows the average frequency-dependent behaviour of experimental and numerical ATFs, obtained by activating all the monopoles for a single corner and performing a root mean square average over all the source-receiver combinations. This representation confirms the previous conclusions: while general frequency trends are well captured by the numerical model, an overestimation of amplitude is visible for the left corner, opposite the microphone array. The comparison between the two numerical cases highlights the expected effect of the ground absorption coefficient: introducing an acoustic absorption on the road surface leads to a general reduction of the ATF amplitudes with respect to the perfectly reflective case, resulting in an improved agreement with the experimental data. This suggests that moderate absorption better represents the actual acoustic behaviour of the test surface.

The spatial trends in terms of overall levels for the four corners averaged over the monopoles [Fig. 11(b)] can be compared with experimental data. It can be observed that the corners located farther from the microphone array exhibit lower ATF amplitudes, confirming that they contribute less to the overall signal. For the corners closer to the array, a generally good agreement is obtained for microphones located near the corner under consideration, whereas the error increases with distance from the source when

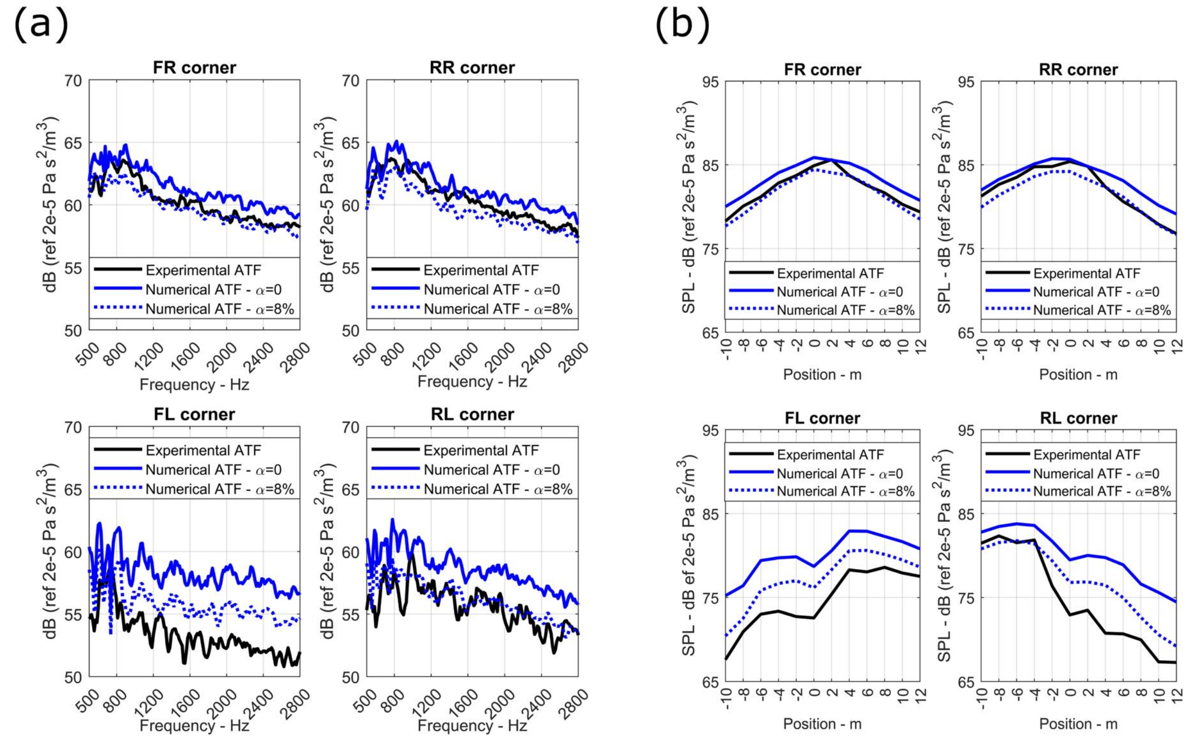

FIG. 11. (a) Experimental vs numerical ATFs averaged per corner, showing frequency trends. (b) Experimental vs numerical OASPL obtained for unit volume acceleration, averaged per corner and evaluated along the microphone array. Black lines correspond to experimental data, while blue lines represent the numerical results with ground absorption coefficients of $\alpha = 0\%$ (solid) and $\alpha = 8\%$ (dashed).

considering $\alpha = 0\%$. In general, the corners farther away from the microphone array exhibit the largest discrepancies with respect to the experimental ATFs. Overall, the comparison highlights that incorporating a realistic ground absorption coefficient improves the consistency of the numerical predictions, although some deviations remain, mainly due to simplified environmental and material assumptions. For example, the wheel arches and the vehicle underbody may have non-negligible acoustic properties, which particularly affect the corners opposite the microphone array.

IV. SOURCE SYNTHESIS AND COAST-BY PREDICTION

The source synthesis methodology had previously been validated by the authors (Dallasta *et al.*, 2025), using experimental ATFs and the same set of monopoles adopted here. That study achieved satisfactory agreement, confirming that both the number and placement of the equivalent sources were appropriate. In this study, the same methodology is used to identify the equivalent monopoles and validate the procedure. However, numerically obtained transfer functions are employed, and measured sound pressure levels at the microphones are used to solve the inverse problem for the equivalent monopoles identification. Consequently, any discrepancies observed in the present analysis are primarily expected to stem from the numerical model used for ATF estimation rather than from limitations in the equivalent source configuration.

Specifically, experimental sound pressure measurements of tire rolling noise were collected at specific receiver locations following the microphone setup described in Sec. II. The 21 microphones on the hemi-circular array were used to perform the source synthesis, while, for validation purposes, 19 additional microphones were employed, extending the assessment of the predicted sound field to a broader set of positions compared to the previous study. Numerical ATFs were evaluated for both sets of microphones employing the indoor model previously described.

The results of the source synthesis methodology in terms of overall sound pressure levels (OASPL) are shown in Fig. 12, comparing the experimentally measured tire rolling noise (black) and the reconstructed response (blue) obtained using the identified monopoles and the numerically computed transfer functions. On the synthesis microphones, the comparison between experimental data and the reconstructed signal demonstrates the effectiveness of the methodology for the inverse problem used to identify the equivalent monopoles. The comparison across the validation microphones allows assessing whether the reconstructed sources correctly reproduce the sound field at locations different from those used for the synthesis, thereby quantifying the error associated with mismatches between numerical and experimental indoor ATFs. This analysis isolates the impact of uncertainties in numerical indoor ATFs, which indicate an average error below 1 dBA across the validation array.

Frequency-dependent trends were further analyzed by performing a sound intensity average over the validation microphones, highlighting errors associated with the use of numerical instead of experimental indoor ATFs.

https://doi.org/10.1121/10.0044578

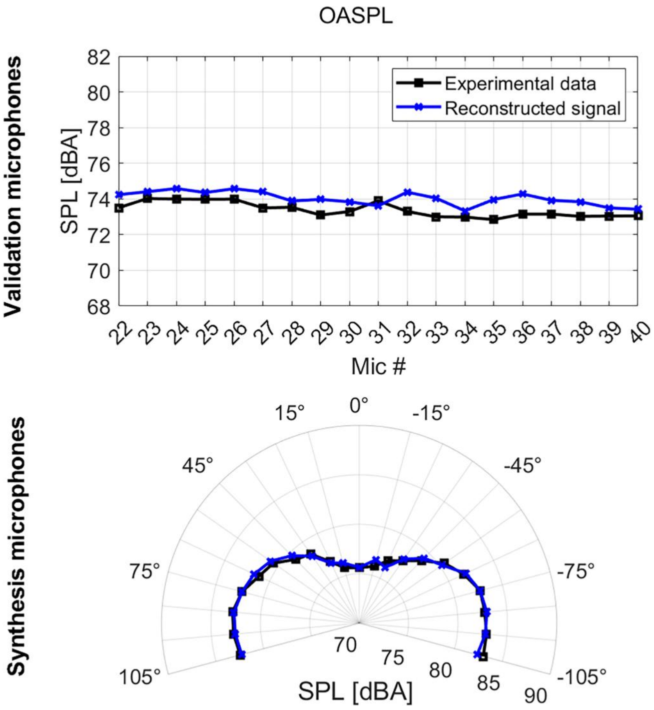

FIG. 12. Validation of the synthesis methodology: OASPL comparison between measured rolling noise (black) and reconstructed response (blue).

The corresponding results are presented both in narrowband and one-third octave band (Fig. 13), comparing the experimental data with the reconstructed signal. While the one-third octave band representation shows similar trends between the two curves, more pronounced deviations are observed in the higher frequency range, particularly from the 1250 Hz central band onwards, due to the increased sensitivity to geometric and boundary details.

Following the identification of the equivalent monopoles from the indoor test rig, the same sources are applied to predict the coast-by sound field. The underlying assumption of the methodology is that the sources synthesized under indoor conditions are representative of those active in outdoor environment.

The coast-by noise prediction was carried out following the methodology described in a previous publication (Dallasta *et al.*, 2026), which accounts for the physical phenomena associated with measuring the sound emitted by a moving source using a stationary microphone, and relies on experimentally measured ATFs. In analogy with the indoor case, in the present study, numerical transfer functions obtained from the model developed in Sec. III were employed. Another advantage of this approach, compared with a fully experimental methodology for the synthesis of the equivalent sources and for the coast-by prediction, lies in the accurate placement of the equivalent sources around the tire footprint, ensuring consistent source positioning between the indoor and outdoor configurations. Furthermore, in the outdoor simulation, the microphones can be precisely positioned to form the array at a distance of 7.5 m from the track centreline to carry out the methodology, thus eliminating any uncertainty related to their spatial arrangement.

The results of the coast-by noise prediction compared with experimental data (black line) are shown in Fig. 14. The prediction was performed using the outdoor numerical transfer functions derived by imposing the two different ground absorption coefficients, namely, $\alpha = 0\%$ (solid blue line) and $\alpha = 8\%$ (dashed blue line). The dispersion band around the numerical average noise levels was obtained by introducing a randomization of the angular positions of the tires across multiple simulation runs, whereas the bands around the experimental curve are the measured dispersion of the experimental test. Both numerical predictions reproduce the overall trend of the experimental data, although some discrepancies in absolute sound pressure levels are observed. On the one hand, the comparison between the two ground absorption coefficients clearly highlights the influence of ground absorption on the predicted coast-by

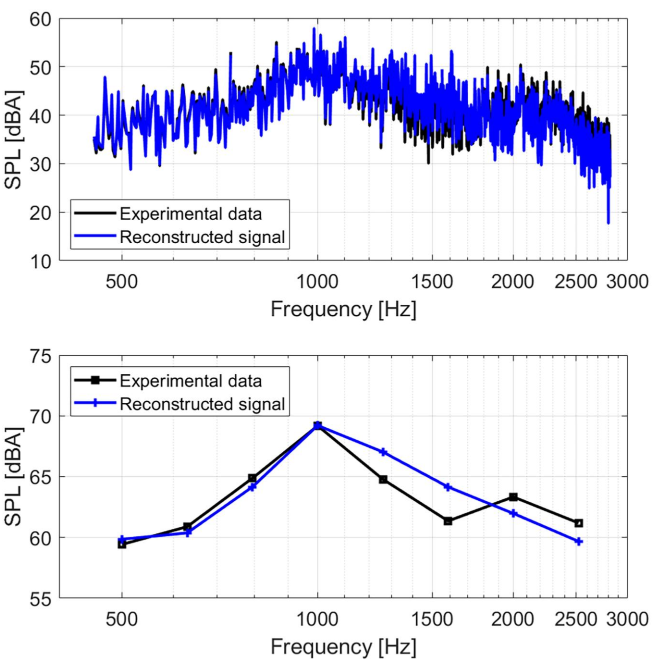

FIG. 13. Averaged frequency-dependent trends over the validation microphones in narrowband results and one-third octave band results.

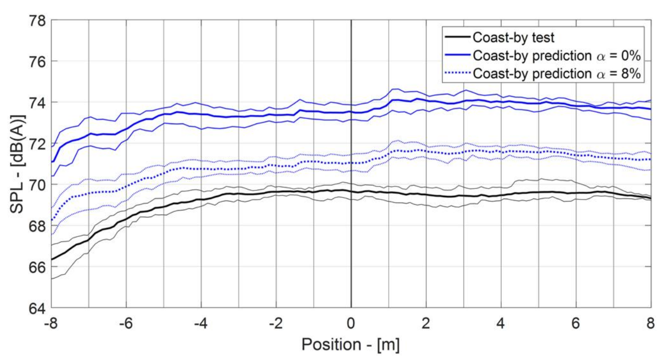

FIG. 14. Coast-by noise level prediction for absorption coefficient $\alpha = 0\%$ and $\alpha = 8\%$, and comparison with experimental data.

noise levels. The simulations show that a variation in α results in SPL differences of up to approximately 2.5 dB(A), demonstrating the sensitivity of coast-by noise levels to the acoustic properties of the test surface. Although only acoustic effects are considered here, these results emphasize the importance of accurately characterizing surface absorptions when performing predictive noise assessments.

When considering the comparison between experimental data and numerical prediction, part of the discrepancies may be attributed to inaccuracies in the numerical models, both under indoor and outdoor conditions. In particular, the indoor validation showed errors at the validation microphones to be attributed to the indoor numerical ATFs. Regarding the ATFs used to represent the outdoor environment, TABLE I showed that also numerical ATFs exhibit modelling errors with respect to the real environment; however, when using an 8% ground absorption coefficient, the ATFs became comparable to the measured ones. Therefore, beyond the uncertainties associated with numerical modelling, differences in tire boundary conditions between indoor and outdoor testing environments can also play a role as observed in Dallasta *et al.* (2026), where a fully-experimental approach was used. Specifically, the indoor characterization relies on drum measurements, whereas the coast-by test is performed on a flat track. Such discrepancies in contact geometry can affect tire excitation and, consequently, the underlying noise generation mechanisms. Moreover, although a road replica reproducing the track used for the coast-by measurements was employed during the indoor campaign, and the tires were subjected to the same loading conditions as in the outdoor setup, variations in surface texture and material composition between the road replica and the actual test track are to be expected.

V. CONCLUSION

This paper discussed the development of numerical models for both indoor and outdoor environments to represent the acoustic behaviour of the testing settings in the framework of tire/road noise prediction through equivalent monopole sources. The resulting models were compared with experimental data collected using a Qsource, to confirm their ability to accurately reproduce the acoustic propagation in both indoor and outdoor environments. For the outdoor scenario, two ground absorption cases, 0% and 8%, were considered. Finally, starting from indoor tire rolling noise measurements, the prediction of coast-by noise due to tire/road interaction is performed. To this purpose, the numerical ATFs were employed both to synthesize equivalent monopole sources and to predict coast-by noise levels. The study further shows that additional uncertainties arise when ATFs are modelled numerically rather than measured experimentally, propagating through the entire prediction chain and how they affect source identification and the reconstructed sound field.

The results highlighted the importance of carefully accounting for modelling assumptions when replacing experimental ATFs with numerical ones, together with the increased modelling complexity of numerical indoor and outdoor representations. Correctly modelling the geometrical features of the environment and the relative spacing between sources and receivers is essential to capture the acoustic behaviour in the relevant frequency range, where higher frequencies require tighter geometric tolerances. In this respect, the use of simplified analytical formulations, particularly hemi-space Green's function models, is unable to reproduce the ATFs frequency trend. The acoustic properties of surfaces must also be included, as it was shown that even moderate absorption of outdoor asphalt can significantly affect the result. The approach used effectively captures the main acoustic phenomena governing coast-by measurements and is suitable for preliminary design evaluations, even though differences in terms of absolute values were observed between predicted and measured coast-by results. On the one hand, they are caused by the inherent approximations of the models; for instance, although the vehicle geometry was reproduced, the acoustic properties of the surfaces, such as the wheel arches and the underbody, were not characterized. Additionally, further improvements could be achieved by compensating for flat-road versus drum-road effects, as changes in contact conditions modify the tire footprint resulting in differences in noise generation and amplification.

In future developments, the numerical framework can be further extended to eliminate the need for experimental sound pressure measurements for the synthesis of the monopoles and to allow direct simulation of the tire rolling under flat conditions. This would require detailed tire rolling noise vibroacoustic models capable of capturing the main tire/road interaction mechanisms. The development and validation of such models constitute future research activity.

ACKNOWLEDGMENTS

This study is part of the AirBorne Exterior Noise (ABEN) research project, carried out in the framework of the Joint Labs cooperation agreement between Politecnico di Milano and Pirelli. The authors gratefully acknowledge Pirelli for providing the support and data necessary for this work.

AUTHOR DECLARATIONS

Conflict of Interest

The authors have no conflicts to disclose.

DATA AVAILABILITY

The data that support the findings of this study are available from Pirelli Tyre S.p.A. Restrictions apply to the availability of these data, which were used under license for this study. Data are available from the authors upon reasonable request and with the permission of Pirelli Tyre S.p.A.

Beckenbauer, T., Klein, P., Hamet, J.-F., and Kropp, W. (**2008**). "Tyre/road noise prediction: A comparison between the SPERoN and HyRoNE models - Part 1," J. Acoust. Soc. Am. **123**, 3388.
Bécot, F. X. (**2003**). "Tyre noise over impedance surfaces—Efficient application of the equivalent sources method," Ph.D. dissertation, Chalmers Tekniska Hogskola, Gothenburg, Sweden.
Behnke, R., and Kaliske, M. (**2015**). "Thermo-mechanically coupled investigation of steady state rolling tires by numerical simulation and experiment," Int. J. Non-Linear Mech. **68**, 101–131.
Campello-Vicente, H., Peral-Orts, R., Campillo-Davo, N., and Velasco-Sanchez, E. (**2017**). "The effect of electric vehicles on urban noise maps," Appl. Acoust. **116**, 59–64.
Dallasta, S., Rapino, L., Ripamonti, F., Baro, S., and Corradi, R. (**2024**). "Accounting for the vehicle influence on tyre noise through acoustic simulation based on equivalent monopole sources," Inter. Noise **270**, 9045–9051.
Dallasta, S., Rapino, L., Ripamonti, F., Baro, S., and Corradi, R. (**2025**). "Tyre/road noise modelling through equivalent monopoles: Source strengths identification based on experimental acoustic transfer functions," Appl. Acoust. **236**, 110719.
Dallasta, S., Rapino, L., Ripamonti, F., Baro, S., and Corradi, R. (**2026**). "Prediction of coast-by tyre/road noise based on equivalent monopoles synthesised from indoor tests," Appl. Acoust. **241**, 111033.
Ding, Y., and Wang, H. (**2019**). "FEM-BEM analysis of tyre-pavement noise on porous asphalt surfaces with different textures," Int. J. Pavement Eng. **20**, 1090–1097.
Dratva, J., Phuleria, H. C., Foraster, M., Gaspoz, J.-M., Keidel, D., Künzli, N., Liu, L.-J. S., Pons, M., Zemp, E., Gerbase, M. W., and Schindler, C. (**2012**). "Transportation noise and blood pressure in a population-based sample of adults," Environ. Health Perspect. **120**, 50–55.
Eisenblaetter, J., Walsh, S. J., and Krylov, V. V. (**2010**). "Air-related mechanisms of noise generation by solid rubber tyres with cavities," Appl. Acoust. **71**, 854–860.
EU (**2020**). *Regulation (EU) 2020/740 of the European Parliament and of the Council of 25 May 2020 on the labelling of tyres with respect to fuel efficiency and other parameters, amending Regulation (EU) 2017/1369 and repealing Regulation (EC) No 1222/2009* (European Union, Brussels, Belgium).
European Commission (**2011**). *Regulation no 117 of the Economic Commission for Europe of the United Nations (UN/ECE) - Uniform provisions concerning the approval of tyres with regard to rolling sound emissions and to adhesion on wet surfaces and/or to rolling resistance* (European Commission, Brussels, Belgium).
Huijssen, J., Fiala, P., Hallez, R., and Desmet, W. (**2010**). "Simulation of pass-by noise of automotive vehicles in the mid-frequency range using Fast Multipole BEM," in *Proceedings of ISMA 2010 - International Conference on Noise and Vibration Engineering, including USD 2010*.
IEA (**2025**). "Global EV Outlook 2025 Paris," https://www.iea.org/reports/global-ev-outlook-2025 (Last viewed 15 November 2025).
ISO (**2019**). *ISO 13325. Coast-by methods for measurement of tyre-to-road sound emission* (International Organization for Standardization, Geneva, Switzerland).
ISO (**2021**). *ISO 10844:2021 Acoustics — Specification of test tracks for measuring sound emitted by road vehicles and their tyres* (International Organization for Standardization, Geneva, Switzerland).
Kim, I., Kim, H., and Kim, Y. (**2023**). "FE-based simulation of radiated noise for a rotating tire," Inter. Noise **268**, 3672–3676.
Kim, S., Jeong, W., Park, Y., and Lee, S. (**2006**). "Prediction method for tire air-pumping noise using a hybrid technique," J. Acoust. Soc. Am. **119**, 3799–3812.
Klein, P., Beckenbauer, T., Hamet, J.-F., and Kropp, W. (**2008**). "Tyre/road noise prediction: A comparison between the SPERoN and HyRoNE models - Part 2," J. Acoust. Soc. Am. **123**, 3389.
Kropp, W., Bécot, F.-X., and Barrelet, S. (**2000**). "On the sound radiation from tyres," Acustica **86**, 769–779.
Kropp, W., Sabiniarz, P., Brick, H., and Beckenbauer, T. (**2012**). "On the sound radiation of a rolling tyre," J. Sound Vib. **331**, 1789–1805.
Lafont, T., Stelzer, R., D'Amico, R., Kropp, W., and Bertolini, C. (**2019**). "Modelling tyre noise in finite element simulations for pass-by noise predictions," Proc. Inst. Mech. Eng. C J. Mech. Eng. Sci. **233**, 6398–6408.
Li, T. (**2018**). "Literature review of tire-pavement interaction noise and reduction approaches," J. Vibroeng. **20**, 2424–2452.
Li, T. (**2019**). "Tire braking/cornering noise analysis: Stick/slip mechanism," in *Proceedings of NoiseCon 2019*, August 26–28, San Diego, CA.
Lui, W. K., and Li, K. M. (**2004**). "A theoretical study for the propagation of rolling noise over a porous road pavement," J. Acoust. Soc. Am. **116**, 313–322.
Meschke, G., Payer, H. J., and Mang, H. A. (**1997**). "3D simulations of automobile tires: Material Modeling, mesh generation, and solution strategies," Tire Sci. Technol. **25**, 154–176.
Nakajima, Y., Inoue, Y., and Ogawa, H. (**1993**). "Application of the boundary element method and modal analysis to tire acoustics problems," Tire Sci. Technol. **21**, 66–90.
Papaioannou, A., Elliott, S. J., and Cheer, J. (**2020**). "Application of ℓ norm regularisation techniques in the synthesis of indoor tyre pass-by noise with the inverse method," J. Sound Vib. **473**, 115240.
Rapino, L., Ripamonti, F., Baro, S., and Corradi, R. (**2024a**). "Numerical analysis of the tread grooves' acoustic resonances for the investigation of tire noise," J. Vib. Acoust. **146**, 041002.
Rapino, L., Ripamonti, F., Dallasta, S., Baro, S., and Corradi, R. (**2024b**). "Synthesis of equivalent sources for tyre/road noise simulation and analysis of the vehicle influence on sound propagation," Appl. Acoust. **216**, 109751.
Sandberg, U. (**2001**). "Tyre/ road noise - Myths and realities," in *Proceedings of Inter-noise 2001*.
Sandberg, U., and Ejsmont, J. A. (**2002**). *Tyre/Road Noise. Reference Book*, Vol. *1* (Informex, Kisa, Sweden), pp. 1–640.
Saraswat, A., Oorath, R., Patel, C., Ghosh, A., Goyal, S., Thomas, J., George, J., Nair, S., and Issac, R. (**2022**). "Tyre-road interaction noise prediction: A simulation-based approach," SAE Technical Papers.
Schutte, J. H., Wijnant, Y. H., and De Boer, A. D. (**2015**). "The influence of the horn effect in tyre/road noise," Acta Acust. united Ac. **101**, 918865.
Song, Y., Xu, L., Li, P., Deng, Z., and Cai, J. (**2026**). "The correlation between brain response and subjective annoyance under natural sound masking of road traffic noise," J. Acoust. Soc. Am. **159**, 157–167.
Wang, X. (**2020**). *Automotive Tire Noise and Vibrations: Analysis, Measurement and Simulation*, Butterworth-Heinemann, Oxford.
Winroth, J., Kropp, W., Hoever, C., Beckenbauer, T., and Männel, M. (**2017**). "Investigating generation mechanisms of tyre/road noise by speed exponent analysis," Appl. Acoust. **115**, 101–108.